ELSEVIER

Journal of Nuclear Materials 275 (1999) 296–304

journal of nuclear materials

www.elsevier.nl/locate/jnucmat

The behaviour of control rod absorber under irradiation

J. Bourgoin[a,*], F. Couvreur[b], D. Gosset[b], F. Defoort[c], M. Monchanin[c], X. Thibault[d]

[a] *Electricité de France, Groupe des Laboratoires, BP23, 37420 Avoine, France*
[b] *CEA-Saclay, Service d'Etude des Matériaux Irradiés, 91191 Gif/Yvette cedex, France*
[c] *Framatome Nuclear Fuel, 10 rue J. Récamier 69456 Lyon cedex 06, France*
[d] *Electricité de France, SEPTEN, 12–14 avenue Dutriévoz, 69628 Villeurbanne, France*

Received 27 November 1998; accepted 20 May 1999

Abstract

Increase of rod diameters and cracking of PWR control rod claddings may occur in operation. In order to understand the contribution of the absorber properties to this damage, EDF and FRAMATOME launched a programme of examinations concerning the silver–indium–cadmium alloy constituting the absorber bars. Density measurements and microstructural investigations such as micrography, microanalysis were carried out in the EDF Hot Laboratory, X-ray diffraction was performed by CEA. The results show that transmutations induce chemical modifications inside the fcc alloy and, further, formation of an hcp phase similar to the ζ phase of the silver alloys. The chemical and crystallographic changes account for the major part of the absorber swelling.

1. Introduction

Control rod claddings may show signs of intergranular cracking in the lower part of the rods under PWR operational conditions. This cracking and the increase in rod diameters constitute a limitation on the life-time of control rod assemblies. Due to 'creep-slump' and swelling (volume increase), the absorber applies a strain on the cladding as shown elsewhere [1,2], both phenomena are dependent on gamma and neutron irradiation conditions.

In order to understand the swelling mechanism of the absorber, EDF and FRAMATOME co-operated to generate a programme of examinations. The latter were carried out in the EDF hot cells at Chinon on control rods coming from 900 MW and 1300 MW reactors. The swelling under irradiation and associated structural changes in the absorber alloy were characterized by means of density measurements, optical microscopy, microanalysis as well as X-ray diffraction (the latter was performed by CEA). This paper details the evolution of the absorber in operation.

2. Material and sampling

The control rod assembly absorber is a bar made of a ternary alloy: Ag (80% wt), In (15% wt) and Cd (5% wt). Before irradiation, the alloy is a solid solution with a face-centered cubic (fcc) crystallographic structure. In operation, the absorber is subjected to gamma rays and to a neutron flux. The gamma rays induce heating; the maximum temperatures obtained (between 300°C and 350°C) are high compared to both recrystallization temperature (~275°C) and melting temperature (~800°C). Thus, 'creep slump' can occur [1] and diffusion kinetics are significant. Inside the absorber bar, the neutron flux exhibits two gradients: along the rod depending on insertion of the Rod Cluster Control Assembly (RCCA) and inside the rod according to absorption laws. Significant swelling due to irradiation defects is not expected regarding to the irradiation temperature which is favorable to damage recovery, but

* Corresponding author.

0022-3115/99/$ - see front matter
PII: S0022-3115(99)00124-5

the temperature and the neutron flux induce a structural change in the alloy [1,3].

All samples were taken from rods, named A (8 cycles) and B (4 cycles), removed from two Rod Cluster Control Assemblies (RCCA's) withdrawn respectively from a 900 MW reactor and from a 1300 MW reactor. It can be noticed that the gamma scanning axial distribution of Rod A (Fig. 1(a)) exhibits a local depression (~10%). This typical feature of a shutdown RCCA corresponds to the top of the fuel pellet stacks where the neutron spectrum and the neutron flux profile are modified. On the contrary, the gamma scanning axial distribution of Rod B (Fig. 1(b)) is monotonic in accordance with profiles usually observed on temperature regulation banks RCCA's (mobile). Therefore, it can be concluded that the stepping movement of the Rod A assembly, belonging to a power regulation bank, was not axially extended during operation.

For density measurements, absorber sections of about 10 mm length (except the lowest one which was ~4 mm long) were sampled along the irradiated length of the rods up to 0.5 m for Rod A and 1 m for Rod B. Some specimens were dedicated to micrography, microanalysis and X-ray diffraction (Table 1). In addition, two samples were used as references (Table 1): firstly, a section of the same bar located in the upper part of the rod where irradiation level is very low and secondly, a section of an unirradiated bar from another heat.

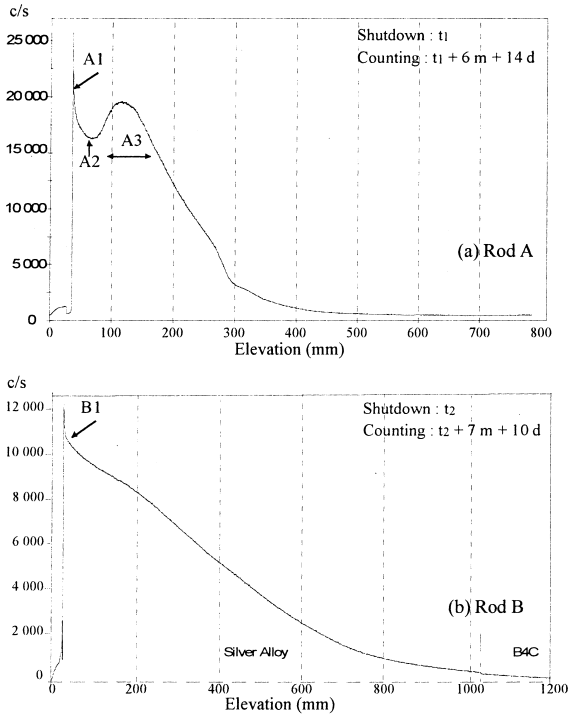

Fig. 1. Gamma scanning profiles of both rods.

3. Results

3.1. Density

Along the absorber bar, the density (Fig. 2) shows a relative decrease of about 1.9% in the lower part of each rod, which is the most irradiated zone. It can be noticed that the minimum in activity of rod A (Fig. 1) has no counterpart on the density profile as shown in Fig. 2. Actually, the neutron spectrum and the neutron flux profile modified in this area involve difference in ratio of physical phenomena i.e., activation and other irradiation effects (transmutations, atom displacements). Thus, there is no linear relationship between activation and the consequences of other irradiation effects as swelling. Anyway, such an effect would be of the same order of

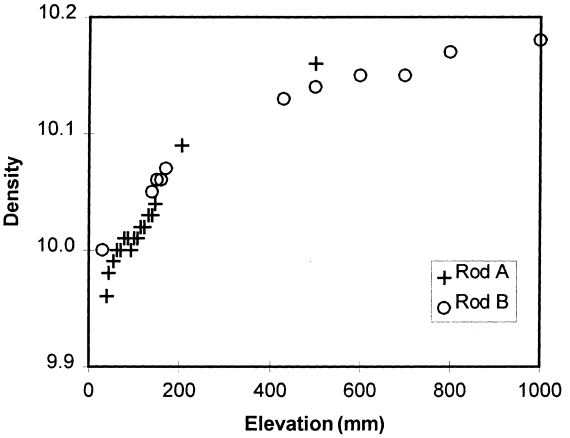

Fig. 2. Evolution of density versus elevation along absorber bars.

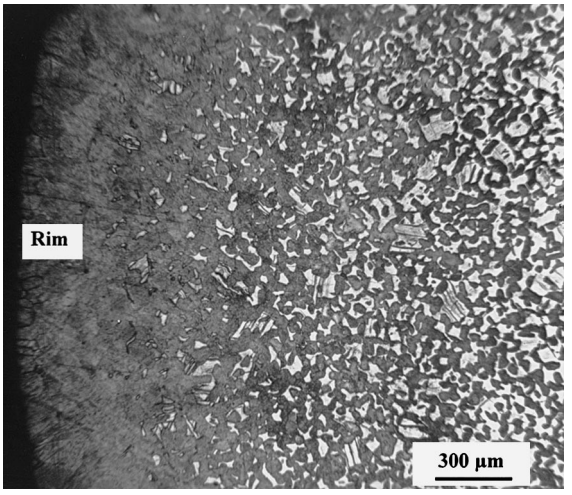

Fig. 3. Micrography of the B1 sample (radial cut).

Table 1
Sampling

Rod	Sample	Elevation on the absorber bar (mm)	Examination[a]
A	A1	35	M, μ
A	A2	55	M, X, μ
A	A3	10 mm cut between 90 and 174	M, X, μ
A	A4	3525	X
B	B1	30	M, μ
–	R0	Reference (unirradiated absorber bar)	X, μ

[a] M = micrography; μ = microanalysis; X = X-ray diffraction.

magnitude than the one of the density measurement uncertainty. The results evidence that the density of the Rod A lower part (~200 mm) is below that of Rod B, due to the higher irradiation in this zone. The increase of bar diameter (swelling – Section 1) can be related to the decrease of density.

3.2. Micrography

Microstructural examinations were carried out in a hot cell with a shielded microscope. Radial sections of the samples named A1, A2, A3, and B1 (Table 1) were observed after polishing and chemical etching. The low magnification micrography in Fig. 3 clearly shows that irradiation drastically modifies the alloy microstructure in accordance with the gradient of neutron irradiation inside the rod thickness. Actually, as illustrated in Fig. 4, a dark phase appears at the grain boundaries of the primary microstucture which is single-phased. Moreover, at the rim (self-shielded zone), the absorber alloy is completely turned into the dark phase in most of the samples.

On all the irradiated samples, the dark phase fraction decreases from the rim to the center of the absorber. To give an estimate of the transformation, image analyses were carried out on micrographs of samples A1 and B1. For both samples, the dark phase content is about 50% at the bar center whereas it is 100% at the rim.

3.3. X-ray diffraction

3.3.1. Method

Sections A2 and A3 (Table 1) were sent to CEA for X-ray diffraction analyses, the first (A2) was located in the depression of the absorber gamma activity and the second (A3) inside the gamma peak. The analyses were performed on a Siemens D500 X-Ray Diffractometer located in a hot cell. In order to correlate the X-ray diffraction spectra to the microanalyses, the samples were polished, perpendicularly to a diameter and, at each selected depth, a diffraction spectrum was recorded. It is worth noting that, given the sample geometry and the beam size (beam width 1 mm, 0.1 entrance slit), the measurements were performed on a surface, the composition of which is not uniform (radial gradient) and the width of which varies with the diffraction angle (Fig. 5). As a consequence, the mean composition of the analysed sample slightly varies on a given spectrum from the small angles (larger composition range) to the large angle lines (composition close to that at the center of the analysed zone). Diffracted lines fitting was performed by

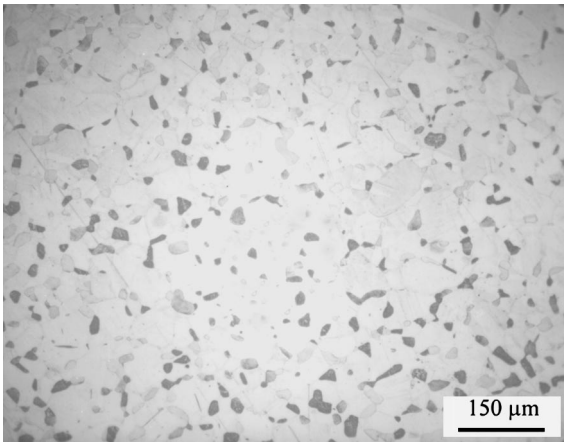

Fig. 4. Micrography of the A2 sample (radial view at 3 mm depth).

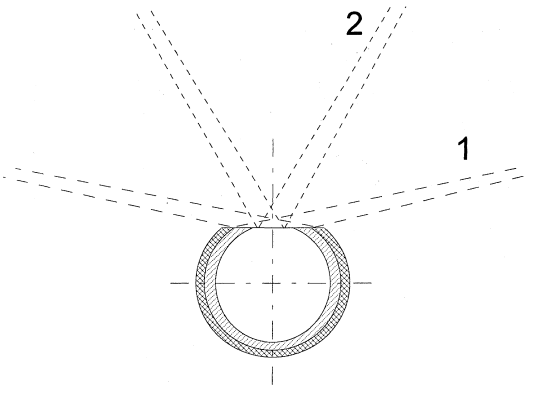

Fig. 5. X-ray analysis: variation of the width of the analysed surfaces with increasing Bragg angle. 1: small diffraction angles; 2: large diffraction angles.

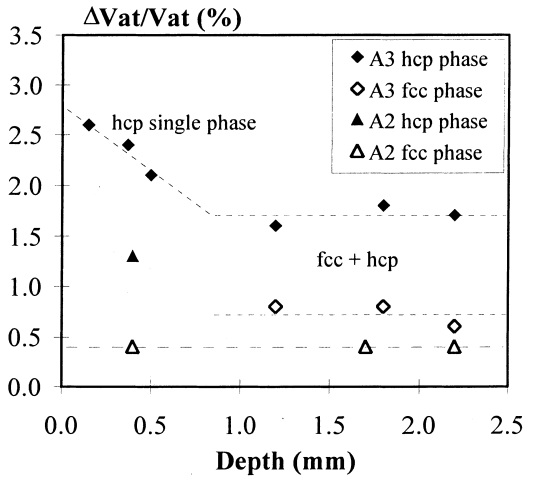

Fig. 6. Evolution of the atomic volume (%) versus depth for the samples A2 and A3 (dotted lines as eye-guides).

using Siemens 'Profile' software and cell parameters were calculated with 'U-FIT' software.

3.3.2. Results

Consistently with micrographies (cf. Section 3.2), X-ray spectra analysis evidences two phases inside the irradiated alloy. The first is similar to the fcc solid solution of the unirradiated alloy (R0 and A4) and it belongs to the Fm3m space group. The second (dark phase Section 3.2), has a close-packed hexagonal lattice (hcp) and belongs to the $P6_3/mmc$ space group; it is similar to the ζ phase of the Ag–In or Ag–Sn binary diagrams (Ag_3X compound type). At the rim, only the hcp phase is identified in specimen A3; its volumic fraction decreases versus depth in the samples.

The atomic volume variation was calculated from phase parameters with respect to the atomic volume of the R0 solid solution. The results given in Table 2 show that irradiation induces an increase of the atomic volume of the fcc phase with respect to the references, furthermore, the atomic volume of the hcp phase is even higher (Table 3).

The atomic volume of the phases is not constant through the depth of a specimen: although the atomic

Table 2
The fcc lattice parameter (a) and atomic volume evolutions

Sample/depth (mm)	a (nm)	Atomic volume (nm^3)	Atomic volume increase (%)[a]
R0	0.41458	0.1781	0
A4/−0.2	0.4146	0.1782	~0
A2/−0.4	0.4152	0.1789	+0.4
A2/−1.7	0.4151	0.1788	+0.4
A2/−2.2	0.4151	0.1788	+0.4
A3/−0.15	No fcc phase		–
A3/−0.37	No fcc phase		–
A3/−0.50	No fcc phase		–
A3/−1.2	0.41576	0.1797	+0.8
A3/−1.8	0.41582	0.1796	+0.8
A3/−2.2	0.41543	0.1792	+0.6

[a] Increase from the atomic volume of the R0 fcc phase.

Table 3
The lattice parameters (a and c) and atomic volume evolutions of the hcp phase

Sample/depth (mm)	a (nm)	c (nm)	Atomic volume (nm^3)	Atomic volume increase[a] (%)
R0	No hcp phase		–	–
A4/−0.2	No hcp phase		–	–
A2/−0.4	0.29480	0.4799	0.18059	+1.3
A2/−1.7	No measurable		–	–
A2/−2.2	No measurable		–	–
A3/−0.15	0.29655	0.48016	0.18285	+2.6
A3/−0.37	0.29648	0.47968	0.1826	+2.4
A3/−0.50	0.29572	0.48012	0.1818	+2.1
A3/−1.2	0.29514	0.47952	0.1809	+1.6
A3/−1.8	0.29544	0.47973	0.1813	+1.8
A3/−2.2	0.29497	0.4807	0.1811	+1.7

[a] Increase from the atomic volume of the R0 fcc phase.

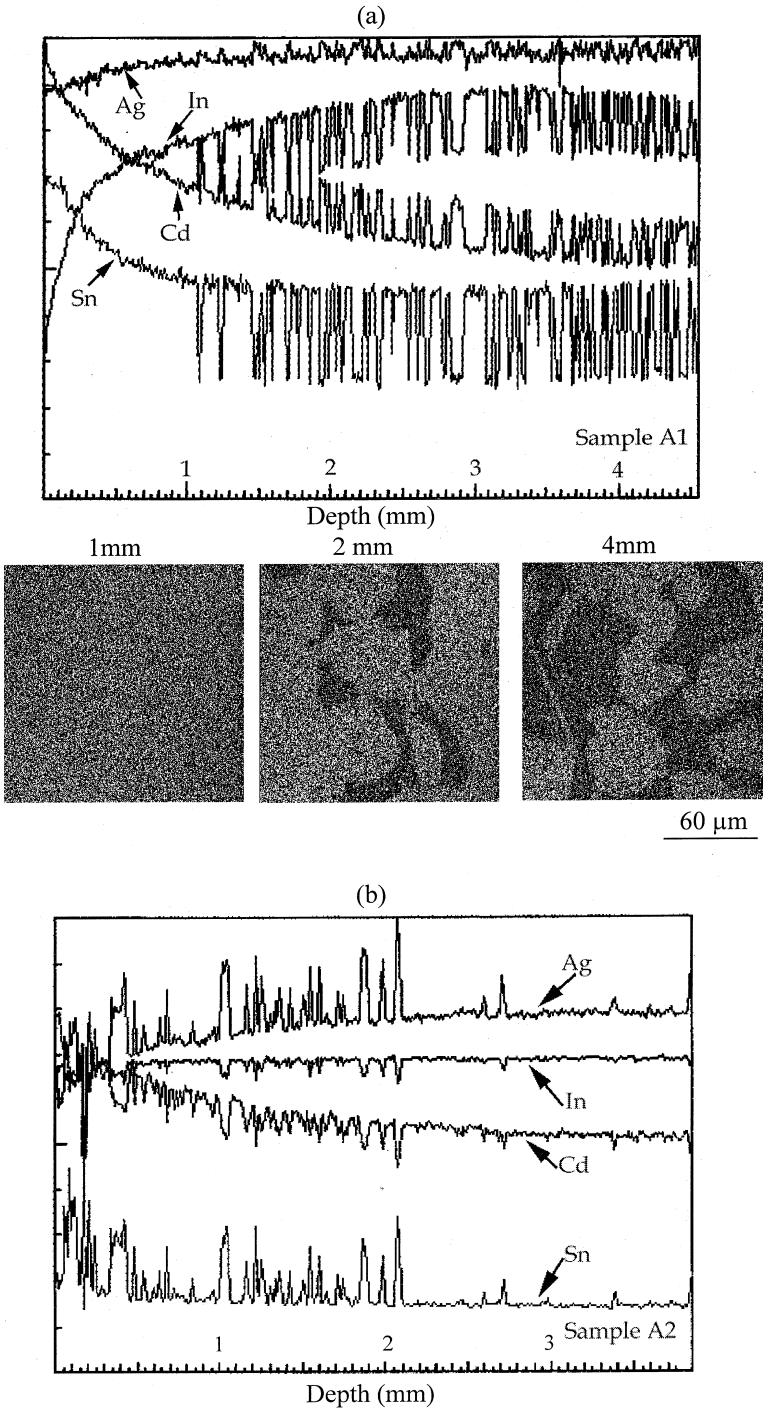

Fig. 7. (a) Qualitative analysis profiles and X-images (Sn) along a radius of the A1 sample, (b) Qualitative analysis profiles along a radius of the A2 sample.

volume of both phases is quite constant inside the two-phase zone, it increases inside the hcp single-phase zone towards the rim (A3) which is more irradiated (Fig. 6). Moreover, inside the two-phase zone, the atomic volume of each phase (hcp and fcc) is higher in sample A3 than in sample A2.

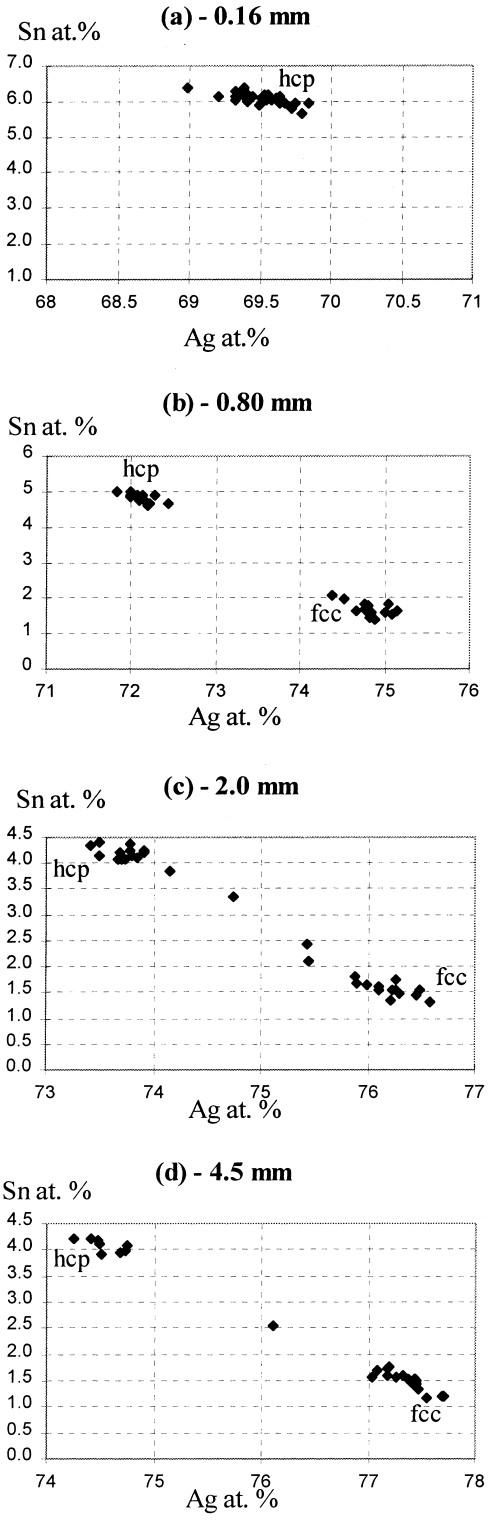

Fig. 8. Ag/Sn correlation results of the A3 sample as a function of depth: (a) 0.16 mm, (b) 0.8 mm, (c) 2 mm, (d) 4.5 mm.

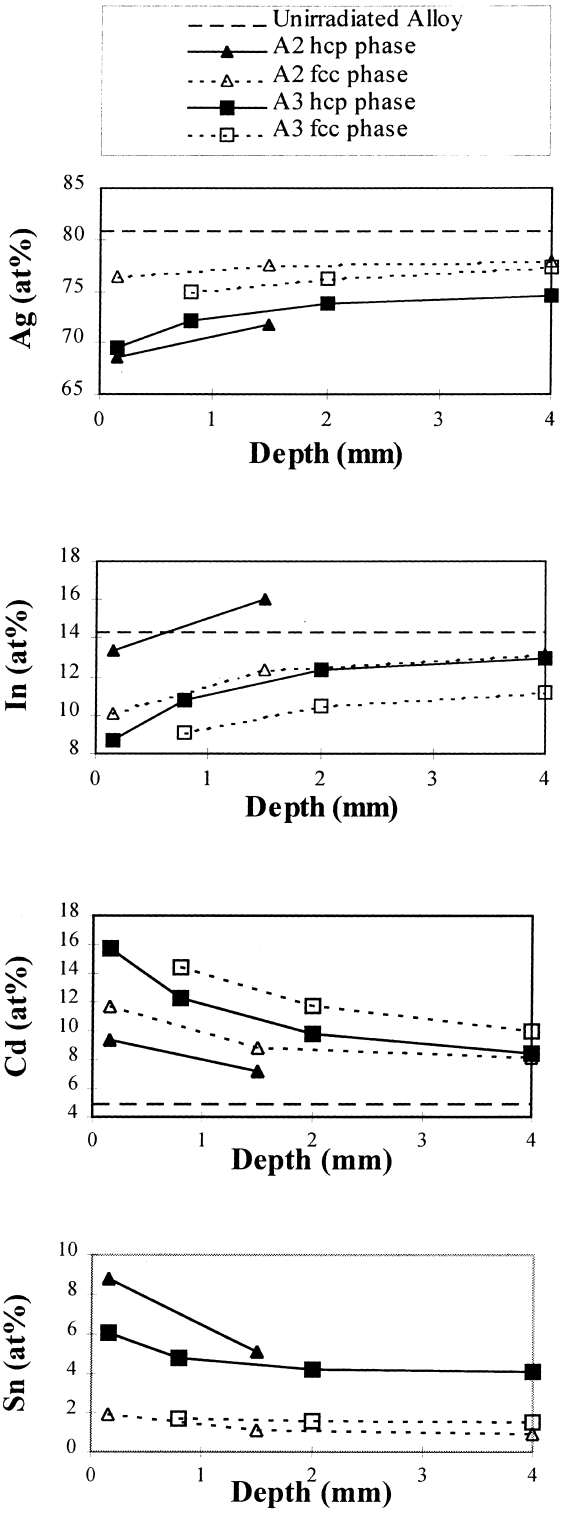

Fig. 9. Radial gradient of element contents in each phase versus depth for the samples A2 and A3.

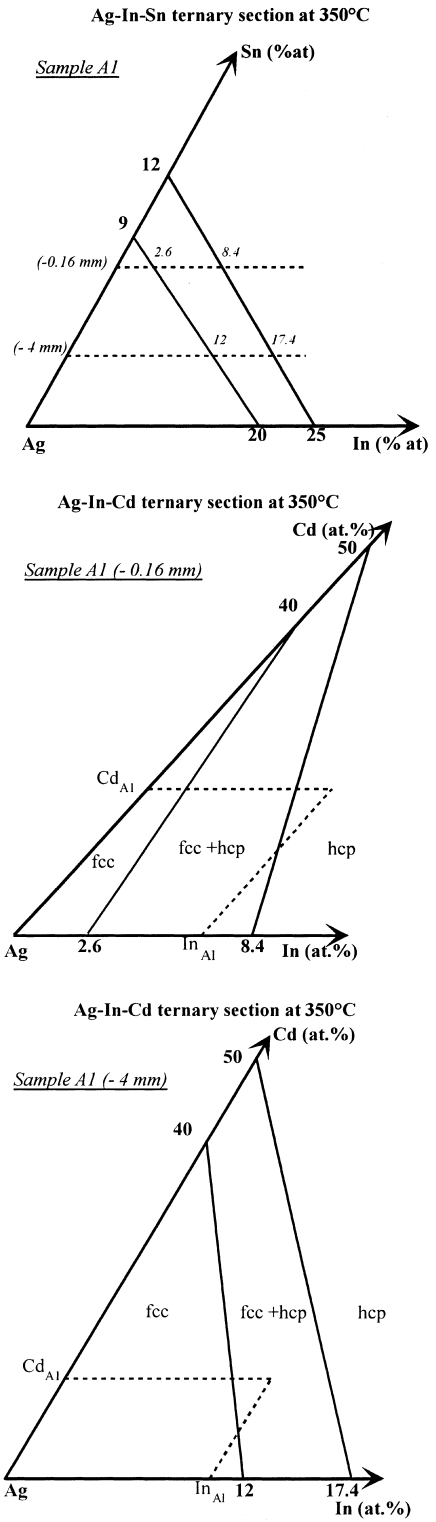

Fig. 10. Microanalysis data of the A1 sample (depths 0.16 and 4 mm) plotted on ternary sections of the quaternary phase diagram at 350°C.

3.4. Microanalysis

3.4.1. Method

Microanalyses were performed inside a CAMEBAX Electron Probe Microanalyser (EPMA) – Microbeam Design; the shielded microanalyser is placed into a hot cell. The standards, made of pure metals (Ag, Cd, In and Sn), were delivered by POLARON. Quantitative analyses were conducted following the ZAF adjustment method. Microanalyses were carried out on polished samples (A1, A2, A3, B1 and R0 – Table 1) without metallographic etching; standards and samples were coated with carbon to improve electric conductivity.

3.4.2. Results

Qualitative elementary analyses plotted on profiles (Fig. 7(a) and (b)) and Sn X mapping (Fig. 7(b)) evidence, in the case of samples A1 and A2, that Sn is present from the rim to the center of the bar. This was observed inside all the irradiated samples. Irradiation transforms the ternary alloy Ag–In–Cd into a quaternary alloy Ag–In–Cd–Sn. The chemical composition of the irradiated alloy exhibits a gradient along the bar radius. Ag and In contents increase from the rim to the center; on the contrary, Cd and Sn contents decrease. Local Ag–Cd and In–Sn associations confirm that a second phase exists (Fig. 7(b)). These results are consistent with X-ray identifications as reported in Section 3.3. Moreover, Ag/Sn correlations, calculated from the quantitative analysis results are presented in Fig. 8 in the case of sample A3. The data on Fig. 8(b) through 8(d) are clearly separated into two distinct populations showing that two phases exist together inside the irradiated alloy. On the contrary, Fig. 8(a) exhibits only one group of dots showing that the rim is only made of hcp phase as illustrated by X-images made on Sn element (Fig. 7(b)). However, in sample A2, the alloy is two-phased throughout the depth (see Fig.7(a)).

As an example, the curves plotted in Fig. 9 show the radial gradient of element contents inside each phase versus depth. The composition gradient of both phases is higher under the surface than at the bar center. Fig. 9 also exhibits the partition of elements between both phases i.e. the tendency of Ag and Cd to be inside the fcc phase and in contrast, the tendency of In and Sn to be inside the hcp phase.

The A2 sample seems to be differentiated since the rim is not completely transformed. In the A2 alloy, In content is higher and conversely, Cd content is lower than the ones the A3 alloy. Furthermore, the hcp phase of this sample has a higher Sn content than in the other samples and a few Sn-rich points were found at the rim inside some hcp phases as noticed elsewhere [1].

4. Discussion

4.1. Irradiation effects on the chemical composition and the microstructure of the alloy

Neutron irradiation of the absorber induces both neutron activations and transmutation reactions inside the absorber [4–6] which can be summarized by the following reactions:

$$Ag \rightarrow Cd,$$
$$In \rightarrow Sn.$$

The transmutations govern the chemistry of the alloy. Irradiation induces Sn creation, the alloy becomes quaternary and the other element contents are modified because of Sn and Cd enrichment and Ag and In depletion. Therefore, the chemical composition of the alloy continuously evolves under irradiation; this leads to metallurgical changes inside the alloy. The primary crystallographic structure is modified on the one hand, by the dilatation of the fcc lattice and, on the other hand, when the solubility limit is reached, by appearance of an hcp phase inside the irradiated alloys. Taking into account the Ag–Cd and In–Sn element associations, this phase could be a compound $[(Ag, Cd)_x (In, Sn)]$ which could be close to the ζ phase of the binary alloys; the hcp atomic volume is larger than the one of the fcc phase. In order to check the consistency of the phase analyses with microstructures, sketches of ternary sections of the quaternary phase diagram were roughly drawn from binary equilibrium diagram at 350°C [7] (Fig. 10). Firstly, the ternary section obtained by joining the solubility limits of Ag–In alloy and Ag–Sn alloy gave an order of magnitude of the In solubility limit which itself was used to draw, at a given Sn content, the Ag–In–Cd ternary sections. Secondly, taking into account the volumic fraction of each phase, the results of microanalyses reported onto these sketches show the consistency of the results obtained on the A1 sample. Beyond the solubility limit, the phase compositions and atomic volume are almost constant and only the hcp phase fraction increases with irradiation. When the two phases exist, their chemical contents and consequently, their atomic volumes, do not vary very much but the mean volume of the material increases since the hcp phase is less compact than the fcc one. In contrast, when the alloy is completely turned into the hcp phase at the rim, chemical composition changes with irradiation fluence, leading to an increase of the lattice parameters and then to an increase of the atomic volume. The results obtained give additional indications on the quaternary diagram Ag–In–Cd–Sn in a temperature range around 300–350°C; as a matter of fact, we can deduce from Fig. 8 that the solubility limit of tin in the fcc phase is around 1.7–2 at.% and the minimum tin content of the hcp phase is about 4 at.%. The few intermediate dots on Fig. 8(c) and (d) could be attributed to a two phase area analysed.

Transmutations induce transformations roughly in accordance with the phase diagrams and the observed gradient of transformation can be attributed to the neutron flux profile along and inside the absorber bar. However, the kinetics of the precipitation process under such conditions exhibits non-classical features as explained in Ref. [8], which could explain the structure singularity observed in the A2 sample.

These changes inside the alloy lead to modifications of its properties such as density, creep rate, which obviously have consequences in absorber behaviour in operation.

4.2. Swelling

We have seen that the chemical and structural modifications that occur under irradiation induce, on the one hand, the increase of the fcc atomic volume and on the other hand the creation of the hcp phase with an even higher atomic volume. Furthermore, by transmutations the average atomic mass of the alloy increases by creation of different heavier isotopes and modifications in atomic composition. Moreover, the reduction of number of atoms by unit volume induces swelling but the

Table 4
Estimation of the average atomic mass (g) of the species of the alloy at the rim of the A3 sample

Element	Unirradiated material	Irradiated material
Ag	107.87	107.81
In	114.82	114.78
Cd	112.42	111.73
Sn	–	115.88

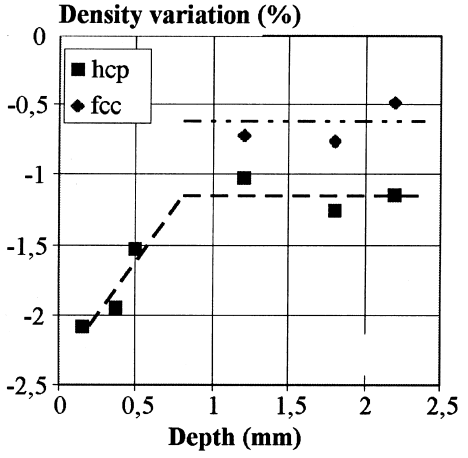

Fig. 11. Assessment of density evolution versus depth (sample A3).

accompanying increase of the average atomic mass of the alloy leads to a smaller variation in density than expected from swelling alone. As an example, the atomic masses of the elements at the rim were evaluated by CEA from a coarse estimation of the neutron absorption cross sections and the neutron spectrum in reactor (Table 4). Taking into account all these facts, as well as the microanalysis data and the phase fractions, the crystallographic density of each phase was estimated (Fig. 11). Both phases are less dense than the primary alloy, and the values of crystallographic density calculated in this way are close to the macroscopic density. However, a difference remains between macroscopic and X-ray density determinations. Actually, density decrease is maximalized by X-ray determinations because of the experimental geometry (X beam width) and the composition gradient of X-ray analysed surface (Fig. 5).

Microstructural evolution of absorber is a phenomenon activated by transmutation reactions and the thermal diffusion of species. As C. Desgranges wrote in Ref. [8]: ''such phenomenon is sensitive [...] to the temperature and to the transmutation yield''. The results show that the absorber swells under irradiation; in the studied range, swelling does not saturate. This is consistent with the large composition range of the hcp phase and with the associated evolution of atomic volume. However, if swelling is inavoidable, density decreasing has never exceeded 2% for the whole population of measurements performed on control rods irradiated up to 9 cycles in a 900 MW reactor.

5. Conclusions

Chemical and structural changes of the Ag–In–Cd ternary alloy under irradiation induce the swelling of the absorber bar in its lower part during operation. These changes are due to the creation of significant contents of tin. In addition to the change of the fcc solid solution parameter, a hcp phase appears, similar to the ζ phase of silver alloys, both contribute to explain the swelling. This phenomenon is complex, it can exhibit singularities and its kinetics depends very closely on irradiation conditions (flux and temperature). Moreover, due to material changes under irradiation, the swelling/creep combination governs the life-time of control rod assemblies.

References

[1] J. Bourgoin, C. Lebuffe, A. Cazus, X. Thibault, M. Monchanin, P.J. Sartor, F. Couvreur, D. Gosset, in: Proceedings of the International Symposium on Contribution of Materials Investigation to the Resolution of Problems Encountered in Pressurised Water Reactors – Fontevraud III, France, September (1994) p. 12.
[2] P.J. Sipush, J. Woodcock, R.W. Chickering, Lifetime of PWR Silver–Indium–Cadmium Control Rods, Electric Power Research Institute Report NP-4512, 1986.
[3] M. Colin, in: Génie Nucléaire B 3 720, Techniques de l'Ingénieur, Paris, 1989, p. 1.
[4] B. Kryger, J.M. Escleine, in: H. Bailly, D. Meinessier, C. Prunier (Eds.), Le combustible nucléaire des réacteurs à eau sous pression et des réacteurs à neutrons rapides, Eyrolles, Paris, 1996, p. 557.
[5] W.L. Zup, J.H. Baard, Nuclear Data Guide for Reactor Neutron Metrology, Netherlands Energy Research foundation, 1979.
[6] R. Pannetier, Vade-mecum du technicien – Table des isotopes, Maisonneuve, Moulins-les-Metz France, 1965.
[7] B. Massalski, Binary Alloy Phase Diagrams, 2nd ed., vol. 1, ASM International, August 1992.
[8] C. Desgranges, G. Martin, F. Defoort, in: Proceedings of the Material Research Society Symposium, Boston, USA, December 2–8, 1996 (MRS,1997).